MANIPULATING SINGLE-MOLECULE EXCIPLEX TADF AND DEEP-BLUE RTP THROUGH NON-COVALENT Π-Π INTERACTION IN A MOLECULAR FOLDAMER

Rongjuan Huang, Kaixin Yu, Shunwei Chen, Kuan Chen, Yanju Luo, Zhiyun Lu, Fernando B. Dias,* and Xujun Zheng**

Dr. R. Huang
Dresden Integrated Center for Applied Physics and Photonic Materials (IAPP), Technische Universität Dresden, Dresden 01069, Germany
K. Yu, K. Chen, Prof. Z. Lu
Key Laboratory of Green Chemistry and Technology (Ministry of Education), College of Chemistry, Sichuan University, Chengdu 610064, P. R. China
E-mail: luzhiyun@scu.edu.cn
Dr. S. Chen
School of Materials Science and Engineering, Qilu University of Technology (Shandong Academy of Sciences), Jinan 250353, P. R. China
Dr. Y. Luo
Analytical & Testing Centre, Sichuan University, Chengdu, 610064, P. R. China
Dr. R. Huang, Prof. F. B. Dias
Physics Department, Durham University, Durham DH1 3LE, UK
E-mail: f.m.b.dias@durham.ac.uk
Dr. X. Zheng
Department of Chemistry, Duke University, Durham, North Carolina 27708, USA
E-mail: xujun.zheng@duke.edu

Keywords: intramolecular non-covalent π-π interactions, single molecule exciplex, thermally activated delayed fluorescence, room temperature phosphorescence, charge transfer character

Abstract: Although the π-π stacking has been widely applied for constructing aggregated emitters in optoelectronics fields, the role of intramolecular non-covalent π-π interactions has not been well studied. Here a supramolecule M-σ-C, with the electron donor (D) and acceptor (A) units spatially separated with a non-covalent bond at a close distance by methylene linker is designed and synthesized. This gives a face-to-face D/A stacking configuration with supramolecular π-π interactions. Temperature-dependent nuclear magnetic resonance measurements and single crystal analyses confirm its folding configuration. In solutions, M-σ-C exhibits a single-molecule exciplex thermally activated delayed fluorescence (TADF) property ascribing to the efficient intramolecular through-space charge transfer (CT) process. While single-molecule deep-blue room temperature phosphorescence (RTP) with a long

afterglow lifetime of 236 ms is observed in a nonpolar matrix, which represents the record lifetime among current ^{3}CT-character featured RTP. This work indicates that the intramolecular non-covalent interactions play an important role in manipulating high-performance single-molecule exciplex TADF and RTP, and provides a feasible molecular design strategy that the knowledges learned from supramolecular chemistry involving into the development of optoelectronic materials.

1. Introduction

Non-covalent intermolecular π-π interaction, which refers to stacking between two π-systems, could regulate the charge transfer (CT) properties between low energy empty orbital and a high-energy filled orbital,[1] playing an important role in many areas of chemistry, material science and biology.[2–6] However, this supramolecular interaction is relatively weak and mainly occurs in crystalline state,[7–11] host-guest systems,[12–14] metal complexes[15] and large clusters,[16] since their entropy and enthalpy effects in these systems are more favorable. Intramolecular non-covalent π-π interaction, especially between donor (D) and acceptor (A) units, is more effective to achieve a smaller entropy-reduction and a larger enthalpy change for a more stable system[17] and crucial for the determination of photophysical properties.[18,19] Although their CT properties can be easily regulated by changing the electron pull-push ability and distance of the D and A π-aromatic units, only limited reports focused on intramolecular non-covalent chromophores,[20,21] which may expand opportunities for investigating their properties at the single molecule level.

In optoelectronics fields, especially for thermally activated delayed fluorescence (TADF) and room temperature phosphorescence (RTP) chromophores, the energy alignment between the singlet (S_1) and triplet (T_1) states with CT or localized excited (LE) character, which is highly associated to the configuration of D and A fragments,[22,23] determines the emission efficiency.[24–26] In these molecules, a proper singlet-triplet energy gap (ΔE_{ST}) is needed that

can be achieved by regulating the spatial overlap of the frontier molecular orbitals of donor and acceptor chromophores;[27–30] meanwhile, a substantial enhanced intersystem crossing (ISC) process and suppressed non-radiative dissipations are crucial, which can be activated by creating a highly rigid environment to suppress the molecular rotations.[31,32] However, the current research into the exploration of the mechanisms in the intramolecular non-covalent π-π supramolecular molecules is still rare, and more attention needs to be paid on designing such molecules with strengthened D/A interactions and comprehensively understanding the role of CT states in regulating single-molecule exciplex (SME) TADF and RTP emission. Based on our current understanding, there are only a few reported cases where the lifetime of ^{3}CT-featured single-molecule organic RTP materials exceeds 100 ms, which hold the potential for practical applications including anti-counterfeiting, information storage, photoelectric devices and gas sensing.[33–35]

Herein, we designed and synthesized a supramolecular foldamer with a D-CH_2(sp^3)-A configuration, namely M-*σ*-C, to investigate the role of intramolecular non-covalent π-π interactions. Compound M-*σ*-C exhibits SME-TADF in solutions and deep-blue SM-RTP at a nonpolar matrix. Carbazole (M)[36,37] and difluorocyanobenzene (C)[38] are chosen as the donor and acceptor units, respectively, which are connected by a non-covalent methylene linker (**Figure 1**). The synthetic procedures and characterizations of M-*σ*-C are presented in **Supporting Information**. Chiral arrangement of compound M-*σ*-C is observed in the single crystal structures (**Figure S5**), both exhibit an intramolecular face-to-face π-π stacking configuration endowed by the flexible methylene linker, with a distance around 3.4 Å. It is within the van der Waals distance, favoring for the intramolecular CT.

2. Results and Discussion

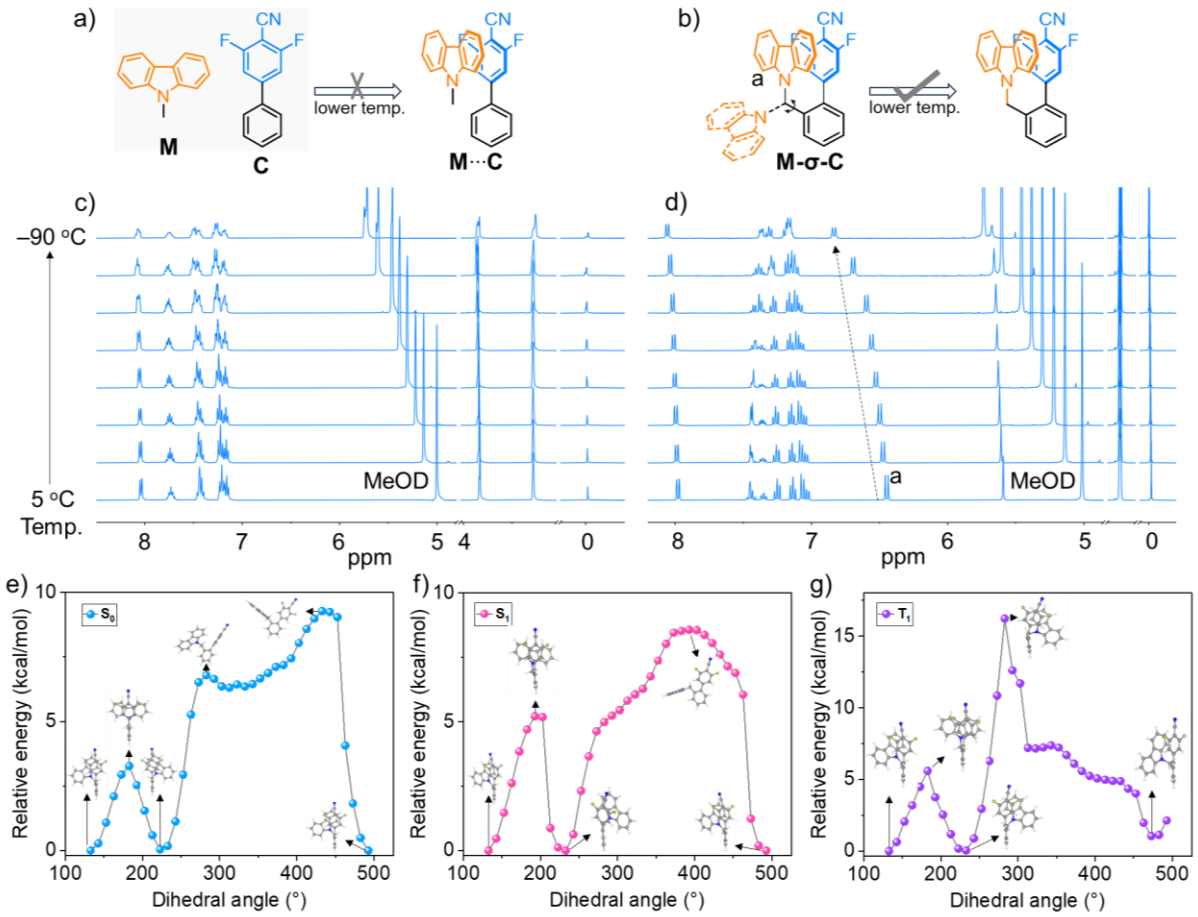

Figure 1. Chemical structures and possible configurations of a) donor and acceptor units and b) M-σ-C at different temperatures. Temperature dependent ^{1}H NMR of c) 1:1 donor and acceptor mixture (M···C) and d) M-σ-C from –90ºC to 5ºC. Potential energy profiles of M-σ-C as a function of N1-C1-C2-C3 dihedral angles at the (e) S_0, (f) S_1 and (g) T_1 states.

The conformation of M-*σ*-C varies with temperature due to the flexible methylene linker as shown in temperature-dependent nuclear magnetic resonance (NMR) measurements. In contrast to the negligible variations in the NMR spectrum observed in the D/A mixture (1:1, M···C) with a random molecular distribution as the temperature changes, M-*σ*-C exhibits a noticeable downfield-shift of its proton H_a (**Figure 1c-d**). This shift occurs because H_a is located in the deshielded region of the π-electron cloud of carbazole, indicating a relatively folded configuration at lower temperatures due to the restrictions on molecular rotations. Besides, the potential energy profiles demonstrate that the π-π stacking is energetically the most stable configuration, as shown in **Figure 1e-g**.

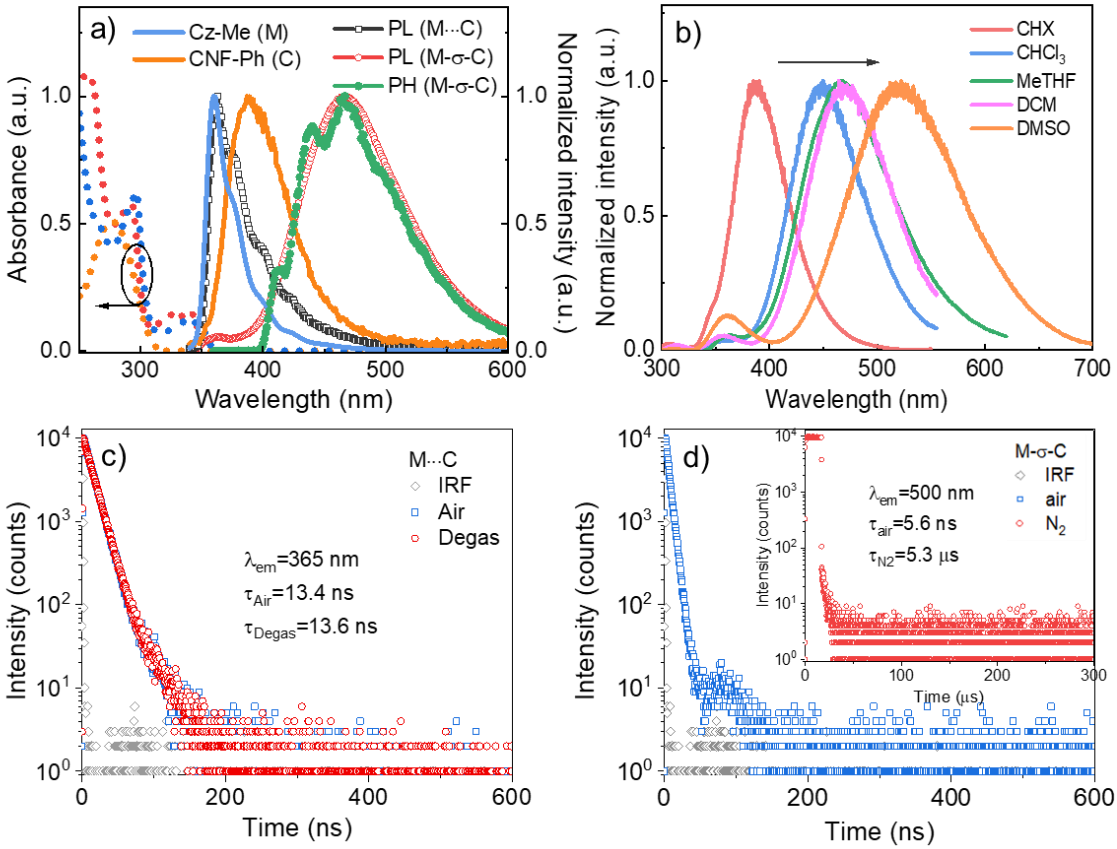

Figure 2. a) Normalized UV-vis absorption and PL spectra of the individual D and A units, M···C and M-*σ*-C at room temperature, phosphorescence spectrum (100 ms, 77 K) of M-*σ*-C in methyl tetrahydrofuran (MeTHF, 1×10^{-5} mol L^{-1}) solution. b) Normalized emission spectra of M-*σ*-C in solvents with different polarities. Time-resolved decay curves of M···C in MeTHF collected at emission of 365 nm and 500 nm, respectively, in air and degassed conditions. d) Time-resolved decay curves of M-σ-C in MeTHF collected at 365 nm in air, inset shows the decay curve at 500 nm in degassed condition. Instrument response function (IRF) is also shown (grey).

The role of intramolecular non-covalent π-π interaction on single-molecule emission in the foldamer M-*σ*-C, here refers to D-A interaction, was first investigated in diluted solutions. **Figure 2a** shows the absorption and photoluminescence (PL) spectra of M-*σ*-C and its individual D and A units in MeTHF solutions. The absorption spectrum of M-*σ*-C has a similar shape with the D unit and shows a slight bathochromic shift with the increasing solvent polarity (**Figure S6**), indicating the possibility of exciplex formation. Two emission bands of M-*σ*-C are observed in MeTHF solution, the weak high-energy band (362 nm) fits well with the donor emission, revealing its localized excited (LE) character; while the low-energy band (466 nm)

exhibits a featureless and red-shifted gaussian shape compared to both D and A emissions, confirming the formation of CT-based exciplex (**Figure 2a**).[39,40] The HOMO and LUMO energies levels of M-*σ*-C were recorded using cyclic voltammetry, which are -5.65 and -2.21 eV, respectively, consistent with those of the individual D and A molecules for exciplex formation (**Figures S7 and 8**). With increasing polarity of solvent, the emission of M-*σ*-C shows a positive solvatochromism, that is, 386 nm in CHX (cyclohexane), 450 nm in DCM (dichloromethane) to 518 nm in DMSO (dimethyl sulfoxide) as depicted in **Figure 2b,** further indicating its S_1 state of CT character.[41] In contrast, the PL spectrum of the D/A physical mixture (M···C) matches well with the D emission peaking at 362 nm, with a broad shoulder contributing from the A unit (**Figure 2a**). It reveals that the emission of M-*σ*-C derives from the intramolecular exciplex, whereas it is hindered in a randomly distributed M···C diluted solution. Moreover, a structural phosphorescence (PH) spectrum of M-*σ*-C was observed in MeTHF solution at 77 K, suggesting T_1 as a ^{3}LE state. Calculated from the onsets of the PL and PH spectra of M-*σ*-C, the energies of the S_1 and T_1 states are estimated to be 3.11 and 3.02 eV, respectively. With such a small ΔE_{ST} of 0.09 eV, the non-covalent M-*σ*-C is favorable to achieve SME-TADF. **Figure 2c** shows that only prompt fluorescence with a short fluorescence lifetime (~13 ns) is observed in both air and degassed M···C solutions. Whereas M-*σ*-C exhibits a short fluorescence lifetime (5.6 ns) in air and longer decay of 5.4 μs in degassed solution (**Figure 2d and S9**). The microsecond range lifetime suggests the triplet exciton harvesting mechanism of intramolecular exciplex DF. The photophysical parameters are summarized in **Table S1**. It is demonstrated that the methylene linker plays an important role in the formation of efficient intramolecular through-space CT interactions between the D and A units, resulting in a radiative decay pathway via the formation of a SME-TADF emission.[39,40]

To regulate singlet-triplet energies for TADF, the behaviors of M-*σ*-C in polar host, DPEPO (bis[2-(diphenylphosphino)phenyl]ether oxide), were also investigated. DPEPO has a high polarity that can lower the singlet state for a small S-T energy gap and a high triplet state (~3.02

eV) avoiding triplet quenching.[42] The high doping ratio of 10 wt% is used to quench the host emission as 1 wt% doping may disturb the study. Different from the PL spectrum in M···C/DPEPO, M-*σ*-C/DPEPO exhibits a broad and gaussian shaped fluorescence spectrum indicating its CT character (**Figure S10a**). Temperature-dependent time-resolved decays were recorded showing three distinct regions (**Figure S10b**): i) prompt fluorescence (PF), independent of temperature in nanosecond range; ii) DF, decaying in microsecond range with a positive temperature dependence; and iii) phosphorescence (PH), noticeable at low temperatures decaying in millisecond time range. At room temperature, M-*σ*-C/DPEPO has a PF lifetime (τ_{PF}) of 18.0 ns and DF lifetime (τ_{DF}) of 42.2 μs (**Figure S11**). The corresponding lifetimes of the three components at different temperatures are summarized in **Table S2**. To better understand the dynamic properties of the emission, the area normalized spectra of M-*σ*-C/DPEPO film at RT and 80 K were recorded. As shown in **Figure S12a**, fluorescence emission progressively shifts to longer wavelengths with increasing delay times, which is associated with the growing contribution of the ^{1}CT emission from ^{1}LE state. ^{1}CT emission remains unchanged at a delay time of 11.2 μs when the face-to-face stacking geometry of the D and A units stabilizes. At 80 K, continuously redshifted spectra are also observed (**Figure S12b**). The stabilized spectrum recorded at delay time of 56.2 ms is identified as the PH emission. Calculated from the onsets of the stabilized spectra, the singlet and triplet energies are estimated to be 3.07 and 2.98 eV, respectively. The small energy gap of 0.09 eV reveals that this non-covalent intramolecular π-π-based foldamer M-*σ*-C could act as a potential TADF emitter in the polar DPEPO matrix. The strictly linear dependence on the laser excitation dose confirms its TADF mechanism (**Figure S13**).

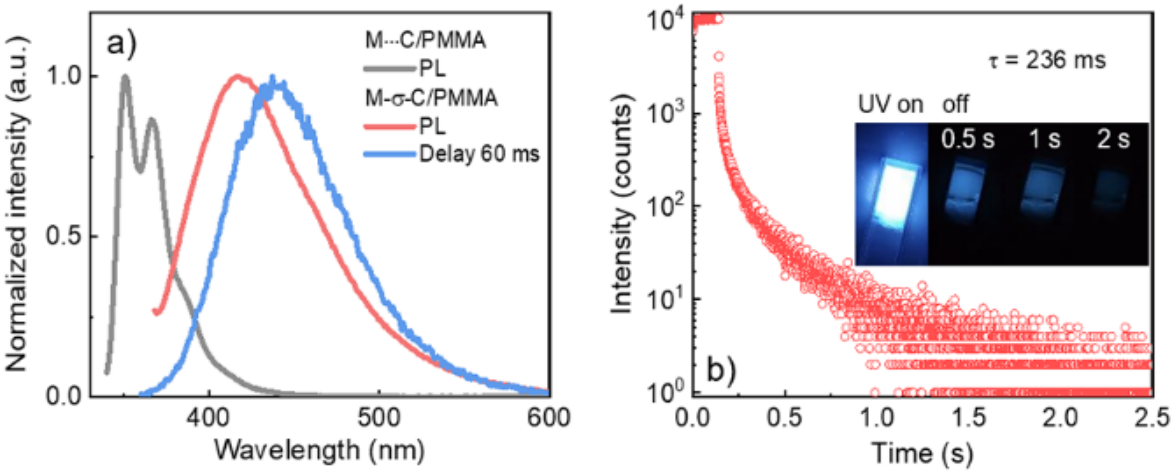

Figure 3. a) Normalized PL (red) and phosphorescence (PH, blue) spectra of 1 wt%M-σ-C/PMMA and PL (grey) of 1 wt%M···C/PMMA films. b) Time-resolved decay curve of 1 wt%M-σ-C/PMMA film collected at 442 nm at ambient condition. Insets: the afterglow photographs taken under and after the removal of 365 nm excitation source.

To further explore the influence of non-covalent intramolecular interactions, the photophysical properties of M-*σ*-C in PMMA (polymethyl methacrylate) matrix (1 wt%) at single-molecule level were investigated. As shown in **Figure 3a**, M···C/PMMA film shows a well-structured LE spectrum, as the molecular distance between the D and A units is relatively large in this system which is unfavorable for CT transition. In contrast, M-*σ*-C/PMMA exhibits a broad PL spectrum with a clear CT feature peaking at 417 nm, indicating the formation of intramolecular exciplex that can undergo intramolecular charge transfer from the D to the A unit. A gaussian shaped deep-blue spectrum peaking at 442 nm was collected at delay time of 60 ms, which can be assigned as RTP from ^{3}CT sate. It can be clearly confirmed by the time-resolved and temperature-dependent spectra (**Figure S14**). This RTP emission may have the contribution of the high-energy ^{3}CT state and the low ^{3}LE state, where the ^{3}LE phosphorescence is covered by the high-energy band tail. With decreasing temperature, the RTP from ^{3}CT phosphorescence shows an increase in intensity and a redshift to a structural spectrum referring to phosphorescence band from ^{3}LE (**Figures S14b and 15**), as it matches well with the phosphorescence spectrum in solution at low temperature (**Figure 2a**). Calculated from the onsets of the phosphorescence of M-σ-C/PMMA film (3.24 eV) and M-σ-C solution (3.02 eV),

the energy gap between ^{3}CT and ^{3}LE is ~ 0.22 eV, which makes the thermal up-conversion possible. The two phosphorescence bands are associated with the thermally activated reverse internal conversion between ^{3}CT and ^{3}LE. The high-energy ^{3}CT phosphorescence shows a relatively slow increase in intensity compared with the ^{3}LE phosphorescence as temperature decreases, as it can no longer be thermally populated efficiently. Moreover, M-*σ*-C/PMMA shows a long-lived lifetime of 236 ms and a deep-blue afterglow after photoactivation at RT (**Figure 3b**). To the best of our knowledge, this represents the record lifetime in single-molecule RTP deriving from ^{3}CT state.[43–46] This can be ascribed to the strong molecular interactions in the nonpolar rigid matrix that effectively block the oxygen permeation and nonradiative decay channels by restricting the molecular vibrations. Notably, the PL and delayed emission (550 nm) in Sigma-Cz based M-σ-C excludes the origination of the phosphorescence from Cz isomer in our synthesized M-σ-C[47] (**Figure S16**).

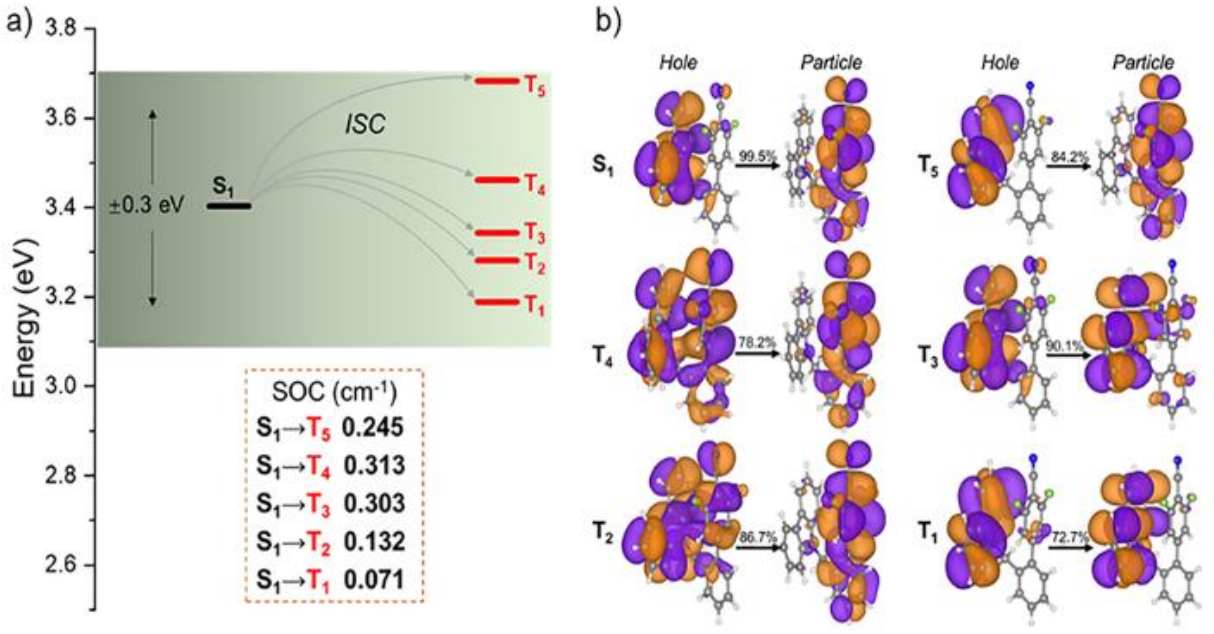

Figure 4. a) Energy levels of S_1, T_1, T_2, T_3, T_4, and T_5 states and SOC values for the ISC process between the excited singlet and triplet states of M-*σ*-C (triplet states having energy difference within 0.3 eV as compared to the S_1 state were considered). b) Main natural transition orbitals (NTOs) describing the excitation characters of the corresponding excited states. The values show the percentage weights of orbital pairs responsible for the excitations.

To gain a deeper insight into the features of the excited states, energy levels, natural transition orbitals (NTOs) and spin-orbit coupling matrix elements (SOCME, ξ) of M-*σ*-C between excited singlet and triplet states were evaluated.[48,49] This non-covalent skeleton endows M-*σ*-C with a spatial separation between the highest occupied molecular orbitals (HOMOs) and the lowest unoccupied molecular orbitals (LUMOs) (**Figure S17**) for TADF; and additionally strengthen intramolecular π-π stacking which can suppress the non-radiative transitions and improve RTP efficiency (**Figure S18**). The small energy gap and large SOC between S_1 and T_n are the two main factors promoting ISC process. **Figure 4a** shows close triplet excited states T_n (n=1–5) to the S_1 state in energy with a small energy difference of no more than 0.3 eV, indicating the existence of multiple ISC channels. The larger SOC constants between the T_n (n=1–5) and S_1 states also confirm the effective ISC process. For instance, it shows an extremely small $\Delta E_{S1–T3}$ of 0.03 eV and large $\xi(S_1–T_3)$ of 0.303 cm^{-1}. The NTO analysis in **Figure 4b** demonstrates that the S_1 state of M-*σ*-C exhibits an obvious CT character with hole and particle wavefunctions localizing on the D and A units, respectively,[50] which is consistent with the CT emission from the S_1 state both in solutions and PMMA film. Whereas in the T_1 state, the hole and particle wavefunctions mainly localize on the D unit indicating a strong LE character, with only a small proportion of the hole wavefunction localizing on the A unit (**Figure S19**). Thus, the T_1 state is dominated by LE character along with a small portion of CT character, and both T_2 and T_4 states have CT character. All these explained the changes of phosphorescence spectra with temperature in M-*σ*-C/PMMA film. The consistent theoretical and experimental results demonstrate that the non-covalent linker in M-*σ*-C could manipulate the SME TADF and RTP properties.

3. Conclusion

In summary, we designed and synthesized a non-covalent D-σ-A structured molecular foldamer M-*σ*-C via a σ-bonded methylene linker. This non-conjugated linker not only breaks the molecular conjugation giving a well-separated HOMO and LUMO distribution, but endows a

face-to-face D/A stacking configuration with abundant supramolecular π-π interactions. Photophysical characterizations reveal M-*σ*-C intramolecular interactions in different existing conditions. It shows a clear SME TADF feature in diluted solutions, which can be ascribed to the effective through space intramolecular CT process. Moreover, a CT-featured deep-blue SM-RTP with a long lifetime up to 236 ms is observed in M-*σ*-C/PMMA film, due to a rigid environment suppressing molecular vibrations and rotations. To the best of our knowledge, this represents the record lifetime of ^{3}CT-featured deep-blue RTP in single-molecule level. By introducing non-covalent π-π interaction to construct supramolecular architectures for optoelectronic applications, this work provides a theoretical principle and practical reference for designing non-covalent emitters to manipulate TADF or RTP properties in different conditions, and brings new thoughts and visions to the material development for optoelectronic multifunctional emitters. Looking ahead, this foldamer can be further used to fabricate the single-molecule fluorescence/phosphorescence diodes. Moreover, the design strategy based on intramolecular non-covalent π-π interaction might enable the possibilities of 1) coupling a given supramolecular architecture to a range of potential material changes; 2) integrating supramolecular knowledge into other scientific disciplines, and finally understanding the mechanisms or phenomena that are not easily emerged or even unobservable.

4. Experimental Section/Methods

Synthesis and Material Characterization: The synthesis details and ^{1}H, ^{13}C and ^{19}F NMR spectra of M-*σ*-C can be found in the Supporting Information. M-*σ*-C were purified by gradient zone sublimation before photophysical characterization.

Sample preparation: Solutions (~10^{-5} M) were prepared in solvents with different polarities and stirred for up to 24 hrs. Films were prepared by drop-casting: PMMA powder (100.0 mg) and M-σ-C powder (1.0 mg) were added into 5 mL toluene and stirred at 50 ^{o}C until blended powders were dissolved to a clear solution. For doped DPEPO film, DPEPO powder (10.0 mg) and M-σ-C powder (1.0 mg) were added into 1 mL toluene and stirred at 50 ^{o}C until blended

powders were dissolved to a clear solution. The mixtures were then drop-casted onto precleaned quartz substrates and annealed at 80 °C and 50 °C for 2 min, respectively.

Cyclic Voltammetry: Electrochemical measurements were performed in solutions of 0.1 M Bu_4NBF_4 (99%, Sigma Aldrich, dried) in 1,2-difluorobenzene (99.9%, Extra Dry, stabilized, AcroSeal®, Acros Organics) at room temperature. Solutions were prepared with 1.0 mM N_2-degassed 1,2-difluorobenzene of M-σ-C. The electrochemical cell is composed of three electrodes: a platinum disc with 1 mm diameter of working area as a working electrode, an Ag/AgCl electrode as a reference electrode and a platinum wire as an auxiliary electrode. All cyclic voltammetry (CV) measurements were performed at room temperature with a potential scan rate of 50 mV/s and calibrated against a ferrocene/ferrocenium (Fc/Fc^+) redox couple. The onset potential was determined from the intersection of two tangents drawn at the rising and background current of the curve. The ionization potential (IP) was calculated from the oxidation (E_{ox}) potential, using the following equation: $IP = E_{ox} + 5.1$. [51] HOMO energy levels were determined using CV analysis by the estimation of IPs which are similar to the HOMO energies. [52] As the reduction potential is out of range, LUMO energies were calculated according to the optical band gap E_g, which was determined from the onset of the UV-vis absorption band.

Photophysical measurements: Steady-state absorption and emission were recorded using a UV-3600 double beam spectrophotometer (Shimadzu) and an Edinburgh FLS980 spectrometer equipped with a white light source and laser light sources, respectively. Photoluminescence quantum yields (QY) were collected on a HORIBA Jobin Yvon Fluorolog-3 fluorescence spectrometer equipped with an integrating sphere (IS80 from Labsphere) and a digital photometer (S370 from UDT) under ambient conditions. The PL decay profiles in air and degassed conditions were measured using a time-correlated single-photon counting (TCSPC) system using a HORIBA Jobin Yvon Fluorolog-3 fluorescence spectrometer, with different excitation sources, 1 MHz LED laser source and spectraLED-355, respectively. Time-resolved decays, fluorescence and phosphorescence spectra were collected by nanosecond gated

luminescence and lifetime measurements (from 400 ps to 1 s) with a high energy pulsed Nd:YAG laser emitting at 355 nm (EKSPLA) by exponentially increasing the gate and delay times. Emission was focused onto a spectrograph equipped with 300 lines/mm grating of 500 nm or 1000 nm base wavelength and detected on a sensitive gated intensified CCD camera (Stanford Computer Optics) with sub nanosecond resolution. Delay times after the trigger pulse and integration time (how long the shutter is open and light is collected) were controlled with up to 0.1 ns accuracy. Temperature-dependent measurements were acquired using a model liquid nitrogen cryostat (Janis Research) and pumping down to *ca.* 10^{-4} mbar vacuum. For initial development of these methods see previously published literature.[53]

The general form of multi-exponential decay formula is shown as below: [54]

$$y = y_0 + A_1 e^{-\frac{t-t_0}{\tau_1}} + A_2 e^{-\frac{t-t_0}{\tau_2}} + A_3 e^{-\frac{t-t_0}{\tau_3}}$$

and the intensity-weighted decay lifetime can be calculated with the following formula:

$$\tau_{\text{int.}} = \frac{A_1\tau_1^2 + A_2\tau_2^2 + A_3\tau_3^3}{A_1\tau_1 + A_2\tau_2 + A_3\tau_3}$$

Here, y_0 is a constant offset that can account for various experimental features (e.g., background intensity level or much longer emission feature that is quasi steady-state in the time window chosen) and t_0 is for compensating slight offsets with respect to the trigger reference.

X-ray crystallography: Single crystal X-ray diffraction M-σ-C is obtained from slow evaporation of ethyl chloroform/acetate/ethanol solution at room temperature and the X-ray diffraction (XRD) are obtained from a Bruker APEX Duo diffractometer through using Mo*K*-α radiation (λ = 0.71073 Å) with a□*ω/2θ* scan mode at the temperature of 298 or 77 K. The single-crystal X-ray structures of M-σ-C were analyzed confirming the supramolecular interactions and molecular packing arrangement.

Quantum chemical calculations: The ground-state (S_0) structure was fully relaxed based on density functional theory (DFT) adopting B3LYP functional and def2-TZVP basis set taking account of D3BJ dispersion correction as implemented in the Gaussian 16 software.[55–58] The

excitations to the excited singlet and triplet states were calculated by the time-dependent DFT (TD-DFT) at the same level of theory based on the relaxed S_0 structure, and the natural transition orbitals (NTOs) were plotted for the interested transitions using the Multiwfn 3.6 software.[48] The spin-orbital coupling (SOC) values for the intersystem crossing (ISC) between excited singlet and triplet states were calculated by the ORCA 5.0.2 program at the same theoretical level.[49] The S_0, S_1 and T_1 potential energy surfaces were investigated by relaxed scan at the B3LYP-D3BJ/6-311G(d,p) level by considering the implicit solvent effect of DMSO by the SMD method using the Gaussian 16 software.[59] The ωB97XD and M06-2X functionals were also used to confirm the accuracy of B3LYP-D3BJ in revealing the charge transfer feature of the excited state in this molecular system.

Supporting Information

Supporting Information is available from the Wiley Online Library or from the author.

Acknowledgements

Dr. R. Huang, K. Yu and Dr. S. Chen contributed equally to this work. This work was financially supported by the MSCA European Postdoctoral Fellowships (Project 101068895) and National Natural Science Foundation of China (No. 12004209).

Conflict of interest

The authors declare no conflict of interest.

Data Availability Statement

The data that support the findings of this study are available from the corresponding author upon reasonable request.

Received: ((will be filled in by the editorial staff))
Revised: ((will be filled in by the editorial staff))
Published online: ((will be filled in by the editorial staff))

References

[1] M. R. Bryce, *Adv. Mater.* **1999**, *11*, 11.

[2] F. Cacialli, J. S. Wilson, J. J. Michels, C. Daniel, C. Silva, R. H. Friend, N. Severin, P. Samori, J. P. Rabe, M. J. O'connell, P. N. Taylor, H. L. Anderson, *Nat. Mater.* **2002**, *1*, 160.

[3] J. Deng, J. Luo, Y. Mao, S. Lai, Y. Gong, D. Zhong, T. Lu, *Sci. Adv.* **2020**, *6*, eaax9976.

[4] N. Meher, P. K. Iyer, *Nanoscale* **2017**, *9*, 7674.

[5] P. Stoliar, R. Kshirsagar, M. Massi, P. Annibale, C. Albonetti, D. M. De Leeuw, F. Biscarini, *J. Am. Chem. Soc.* **2007**, *129*, 6477.

[6] C. Demangeat, Y. Dou, B. Hu, Y. Bretonnière, C. Andraud, A. D'Aléo, J. W. Wu, E. Kim, T. Le Bahers, A. Attias, *Angew. Chem. Int. Ed.* **2021**, *60*, 2446.

[7] I. Bhattacharjee, S. Hirata, I. Bhattacharjee, S. Hirata, *Adv. Mater.* **2020**, *32*, 2001348.

[8] N. Gan, X. Wang, H. Ma, A. Lv, H. Wang, Q. Wang, M. Gu, S. Cai, Y. Zhang, L. Fu, M. Zhang, C. Dong, W. Yao, H. Shi, Z. An, W. Huang, *Angew. Chem. Int. Ed.* **2019**, *58*, 14140.

[9] G. Li, D. Jiang, G. Shan, W. Song, J. Tong, D. Kang, B. Hou, Y. Mu, K. Shao, Y. Geng, X. Wang, Z. Su, *Angew. Chem. Int. Ed.* **2022**, *61*, e202113425.

[10] A. S. Mikherdov, A. S. Novikov, V. P. Boyarskiy, V. Y. Kukushkin, *Nat. Commun.* **2020**, *11*, 2921.

[11] L. Sun, W. Zhu, X. Zhang, L. Li, H. Dong, W. Hu, *J. Am. Chem. Soc.* **2021**, *143*, 19243.

[12] Z. Yuan, J. Wang, L. Chen, L. Zou, X. Gong, X. Ma, *CCS Chem.* **2020**, *2*, 158.

[13] X. Zhang, L. Du, W. Zhao, Z. Zhao, Y. Xiong, X. He, P. F. Gao, P. Alam, C. Wang, Z. Li, J. Leng, J. Liu, C. Zhou, J. W. Y. Lam, D. L. Phillips, G. Zhang, B. Z. Tang, *Nat. Commun.* **2019**, *10*, 5161.

[14] F. Xiao, H. Gao, Y. Lei, W. Dai, M. Liu, X. Zheng, Z. Cai, X. Huang, H. Wu, D. Ding, *Nat. Commun.* **2022**, *13*, 186.

[15] O. Yamauchi, *Phys. Sci. Rev.* **2016**, *1*, 20160001.

[16] J. Mei, N. L. C. Leung, R. T. K. Kwok, J. W. Y. Lam, B. Tang, *Chem. Rev.* **2015**, *115*, 11718.

[17] M. Liu, X. Han, H. Chen, Q. Peng, H. Huang, *Nat. Commun.* **2023**, *14*, 2500.

[18] P. Li, E. C. Vik, K. D. Shimizu, *Acc. Chem. Res.* **2020**, *53*, 2705.

[19] N. E. Jackson, B. M. Savoie, K. L. Kohlstedt, M. Olvera De La Cruz, G. C. Schatz, L. X. Chen, M. A. Ratner, *J. Am. Chem. Soc.* **2013**, *135*, 10475.

[20] X. K. Chen, B. W. Bakr, M. Auffray, Y. Tsuchiya, C. D. Sherrill, C. Adachi, J. L. Bredas, *J. Phys. Chem. Lett.* **2019**, *10*, 3260.

[21] Z. Yin, M. Gu, H. Ma, X. Jiang, J. Zhi, Y. Wang, H. Yang, W. Zhu, Z. An, *Angew. Chem. Int. Ed.* **2020**, *60*, 2058.

[22] J. Yang, X. Zhen, B. Wang, X. Gao, Z. Ren, J. Wang, Y. Xie, J. Li, Q. Peng, K. Pu, Z. Li, *Nat. Commun.* **2018**, *9*, 840.

[23] S. Garain, S. Kuila, B. C. Garain, M. Kataria, A. Borah, S. K. Pati, S. J. George, *Angew. Chem. Int. Ed.* **2021**, *60*, 12323.

[24] C. Chen, R. Huang, A. S. Batsanov, P. Pander, Y. T. Hsu, Z. Chi, F. B. Dias, M. R. Bryce, *Angew. Chem. Int. Ed.* **2018**, *57*, 16407.

[25] R. Huang, N. A. Kukhta, J. S. Ward, A. Danos, A. S. Batsanov, M. R. Bryce, F. B. Dias, *J. Mater. Chem. C* **2019**, *7*, 13224.

[26] N. A. Kukhta, R. Huang, A. S. Batsanov, M. R. Bryce, F. B. Dias, *J. Phys. Chem. C* **2019**, *123*, 26536.

[27] R. Braveenth, K.-Y. Chai, *Materials* **2019**, *12*, 2646.

[28] T. A. Lin, T. Chatterjee, W. L. Tsai, W. K. Lee, M. J. Wu, M. Jiao, K. C. Pan, C. L. Yi, C. L. Chung, K. T. Wong, C. C. Wu, *Adv. Mater.* **2016**, *28*, 6976.

[29] M. Colella, A. Danos, A. P. Monkman, *J. Phys. Chem. Lett.* **2019**, *10*, 793.

[30] T. C. Lin, M. Sarma, Y. T. Chen, S. H. Liu, K. T. Lin, P. Y. Chiang, W. T. Chuang, Y. C. Liu, H. F. Hsu, W. Y. Hung, W. C. Tang, K. T. Wong, P. T. Chou, *Nat. Commun.* **2018**, *9*, 3111.

[31] Y. Yang, Y. Liang, Y. Zheng, J. Li, S. Wu, H. Zhang, T. Huang, S. Luo, C. Liu, G. Shi, F. Sun, Z. Chi, B. Xu, *Angew. Chem. Int. Ed.* **2022**, *61*, e202201820.

[32] X. Dou, T. Zhu, Z. Wang, W. Sun, Y. Lai, K. Sui, Y. Tan, Y. Zhang, W. Z. Yuan, *Adv. Mater.* **2020**, *32*, 2004768.

[33] L. Deng, Z. Ma, J. Zhou, L. Chen, J. Wang, X. Qiao, D. Hu, D. Ma, J. Peng, Y. Ma, *Chem. Eng. J.* **2022**, *449*, 137834.

[34] T. Wang, J. De, S. Wu, A. K. Gupta, E. Zysman-Colman, *Angew. Chem. Int. Ed.* **2022**, *61*, e202206681.

[35] W. Sun, Z. Wang, T. Wang, L. Yang, J. Jiang, X. Zhang, Y. Luo, G. Zhang, *J. Phys. Chem. A* **2017**, *121*, 4225.

[36] Y. Xiong, Z. Zhao, W. Zhao, H. Ma, Q. Peng, Z. He, X. Zhang, Y. Chen, X. He, J. W. Y. Lam, B. Tang, *Angew. Chem. Int. Ed.* **2018**, *57*, 7997.

[37] K. Zheng, X. Yang, F. Ni, Z. Chen, C. Zhong, C. Yang, *Chem. Eng. J.* **2020**, *408*, 127309.

[38] X. Zheng, R. Huang, C. Zhong, G. Xie, W. Ning, M. Huang, F. Ni, F. B. Dias, C. Yang, *Adv. Sci.* **2020**, *7*, 1902087.

[39] D. W. Cho, M. Fujitsuka, K. H. Choi, M. J. Park, U. C. Yoon, T. Majima, *J. Phys. Chem. B* **2006**, *110*, 4576.

[40] N. Mataga, H. Chosrowjan, S. Taniguchi, *J. Photochem. Photobiol. C: Photochem. Rev.* **2005**, *6*, 37.

[41] X. Tang, L. Cui, H. Li, A. J. Gillett, F. Auras, Y. Qu, C. Zhong, S. T. E. Jones, Z. Jiang, R. H. Friend, L. Liao, *Nat. Mater.* **2020**, *19*, 1332.

[42] J. Zhang, D. Ding, Y. Wei, H. Xu, *Chem. Sci.* **2016**, *7*, 2870.

[43] S. Garain, S. N. Ansari, A. A. Kongasseri, B. C. Garain, S. K. Pati, S. J. George, *Chem. Sci.* **2022**, *13*, 10011.

[44] A. A. Kongasseri, S. N. Ansari, S. Garain, S. M. Wagalgave, S. J. George, *Chem. Sci.* **2023**, *14*, 12548.

[45] S. Garain, S. M. Wagalgave, A. A. Kongasseri, B. C. Garain, S. N. Ansari, G. Sardar, D. Kabra, S. K. Pati, S. J. George, *J. Am. Chem. Soc.* **2022**, *144*, 10854.

[46] K. Chen, Y. Luo, M. Sun, C. Liu, M. Jia, C. Fu, X. Shen, C. Li, X. Zheng, X. Pu, Y. Huang, Z. Lu, *Angew. Chem. Int. Ed.* **2023**, e202314447.

[47] C. Chen, Z. Chi, K. C. Chong, A. S. Batsanov, Z. Yang, Z. Mao, Z. Yang, B. Liu, *Nat. Mater.* **2020**, *20*, 175.

[48] T. Lu, F. Chen, *J. Comput. Chem.* **2012**, *33*, 580.

[49] F. Neese, *WIREs Comput. Mol. Sci.* **2012**, *2*, 73.

[50] L. Cui, A. J. Gillett, S. Zhang, H. Ye, Y. Liu, X. Chen, Z. Lin, E. W. Evans, W. K. Myers, T. K. Ronson, H. Nakanotani, S. Reineke, J. L. Bredas, C. Adachi, R. H. Friend, *Nat. Photon.* **2020**, *14*, 636.

[51] C. M. Cardona, W. Li, A. E. Kaifer, D. Stockdale, G. C. Bazan, *Adv. Mater*. **2011**, *23*, 2367.

[52] P. Data, R. Motyka, M. Lapkowski, J. Suwinski, A. P. Monkman, *J. Phys. Chem. C* **2015**, *119*, 20188.

[53] C. Rothe, A. P. Monkman, *Phys. Rev. B: Condens. Matter Mater. Phys.* **2003**, *68*, 075208.

[54] J. Enderlein, R. Erdmann. *Opt. Commun.* **1997**, *134*, 371.

[55] F. Weigend, R. Ahlrichs, *Phys. Chem. Chem. Phys.* **2005**, *7*, 3297.

[56] A. D. Becke, *J. Chem. Phys.* **1993**, *98*, 5648.

[57] S. Grimme, S. Ehrlich, L. Goerigk, *J. Comput. Chem.* **2011**, *32*, 1456.

[58] M. J. Frisch, G. W. Trucks, H. B. Schlegel, G. E. Scuseria, M. A. Robb, J. R. Cheeseman, G. Scalmani, V. Barone, G. A. Petersson, H. Nakatsuji, X. Li, M. Caricato, A. V.

Marenich, J. Bloino, B. G. Janesko, R. Gomperts, B. Mennucci, H. P. Hratchian, J. V. Ortiz, A. F. Izmaylov, J. L. Sonnenberg, D. Williams-Young, F. Ding, F. Lipparini, F. , G. J. Egidi, B. Peng, A. Petrone, T. Henderson, D. Ranasinghe, V. G. Zakrzewski, J. Gao, N. Rega, G. Zheng, W. Liang, M. Hada, M. Ehara, K. Toyota, R. Fukuda, J. Hasegawa, M. Ishida, T. Nakajima, Y. Honda, O. Kitao, H. Nakai, T. Vreven, K. Throssell, J. A. Montgomery Jr., J. E. Peralta, F. Ogliaro, M. J. Bearpark, J. J. Heyd, E. N. Brothers, K. N. Kudin, V. N. Staroverov, T. A. Keith, R. Kobayashi, J. Normand, K. Raghavachari, A. P. Rendell, J. C. Burant, S. S. Iyengar, J. Tomasi, M. Cossi, J. M. Millam, M. Klene, C. Adamo, R. Cammi, J. W. Ochterski, R. L. Martin, K. Morokuma, O. Farkas, J. B. Foresman, D. J. Fox, *Gaussian, Inc., Wallingford CT,* **2016**. *GaussView 5.0. Wallingford, E.U.A.*

[59] M. J. Frisch, J. A. Pople, J Stephen Binkley, *J. Chem. Phys.* **1984**, *80*, 3265.

Rongjuan Huang, Kaixin Yu, Shunwei Chen, Kuan Chen, Yanju Luo, Zhiyun Lu,* Fernando B. Dias,* and Xujun Zheng*

Manipulating Single-Molecule Exciplex TADF and Deep-Blue RTP Through Non-Covalent π-π Interaction in a Molecular Foldamer

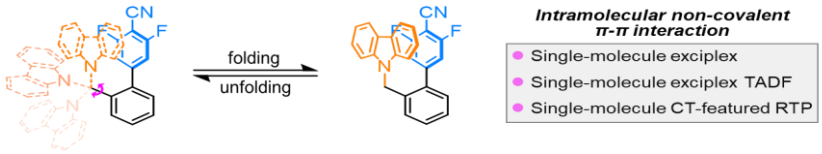

We broaden the application of intramolecular non-covalent π-π interactions to the realm of single-molecule optoelectronic emitters, by featuring a face-to-face donor/acceptor stacking configuration with efficient through-space charge transfer. The resulting supramolecular foldamer showcase the high-performance single-molecule exciplex thermally activated delayed fluorescence and demonstrated a record lifetime of 236 milliseconds for single-molecule deep-blue room temperature phosphorescence with charge transfer feature.